A Deadbeat PI Controller With Modified Feedforward for PMSM Under Low Carrier Ratio

ZHIJIAN ZHANG[1], **LONG JING**[1], **XUEZHI WU**[1,2], **(Member, IEEE)**,
WENZHENG XU[1], **JINGDOU LIU**[1], **GEGE LYU**[1], **AND ZILIAN FAN**[1]

[1]National Active Distribution Network Technology Research Center, Beijing Jiaotong University, Beijing 100044, China
[2]Collaborative Innovation Center of Electric Vehicles in Beijing, Beijing Jiaotong University, Beijing 100044, China

Corresponding author: Long Jing (ljing@bjtu.edu.cn)

ABSTRACT When the permanent magnet synchronous motor (PMSM) operates at low carrier ratio, the decoupling capability and dynamic performance of the proportional-integral (PI) controller are limited by the digitization delay. In this paper, a deadbeat PI controller is proposed by modified the feedforward. With the modified feedforward, the open-loop transfer function can eliminate imaginary components. Thereby the full decoupling of d and q is realized. At the same time, the controller also has full control over the location of the closed-loop poles, indicating that it can have a deadbeat response for the command tracking. For the disturbance rejection, the controller allows us to select the speed with which the controller can cancel the effect of a disturbance. Further considering that the motor parameters are inaccurate, by designing the controller coefficients with the maximum value of the closed-loop poles, the current-loop can ensure the dynamic performance and harmonic suppression ability. Finally, the effectiveness of the proposed controller is verified by the simulations and experiments.

INDEX TERMS PMSM, low carrier ratio, the PI controller, dynamic performance, decoupling capability.

I. INTRODUCTION

PMSM has attracted more and more attention in the fields of industry, household appliances, and electric vehicles because of its various advantages compared with asynchronous motors, such as high efficiency, high power density, and high reliability [1], [2]. In particular, the railway system driven by PMSM is becoming increasingly popular because of the high density and wide speed range [3]. In a high-power traction and drive system, the speed of motors is high to meet the traction requirement [4], while the switching frequency of the inverter can only reach a few hundred Hertz to reduce the power loss of power devices [5], [6]. In the above case, the ratio of the sampling frequency over the fundamental frequency of the PMSM is very small. As a result, the PMSM impedance-coupling in Synchronous Reference Frame (SRF) and the time-delay inherent in the digital control system occupy a larger proportion because of high speed and low frequency, respectively [7]–[9]. For improving the dynamic performance of the current when the PMSM operates at low carrier ratio, the current controller needs to be further studied.

The associate editor coordinating the review of this manuscript and approving it for publication was Atif Iqbal[ID].

At present, the widely-used current controller is the PI controller in SRF, which can achieve zero tracking error of the fundamental frequency [10]. To improve decoupling capability and dynamic performance, the feedforward is introduced into the PI controller [11]. To improve the robustness to parameter changes, an extended state observer is used to compensate the disturbance caused by the change of inductance parameters and current coupling in [12], and it allows the current loop regulator to a linear link. However, when the PMSM works at low carrier ratio, computation and modulation imply an additional delay of one and a half samples in the stationary frame $G_d(s) = e^{-1.5sT_s}$ [13], where T_s is the switching period. Therefore, it is difficult for the observer to realize the real-time compensation of the disturbance in the dynamic process, and the decoupling capacity of the d and q axes needs further study.

As a result, lots of researches have been carried out for the performance improvement of the current loop at low carrier ratio. In [14], the phase leading angle is added into the Park inverse transformation to compensate for the digital delay, which can ensure the stability of the drive system. The controller is simple and easy to be implemented, but its

decoupling capability is not taken into consideration in the paper. Therefore, a complex vector PI controller based on the pole-zero cancellation is proposed in [15], which has better decoupling performance and parameter robustness at high-speed. However, the controller suffers from poor disturbance rejection at low frequency, and it needs to be overcome by the active resistance properties [16]. The methods proposed above are designed in the continuous domain, and the digital implementation will reduce the dynamic performance when it operates at low carrier ratio [17]. Moreover, it is convenient to consider the time-delay and Zero-Order Holder (ZOH) in the discrete domain. Therefore, a discrete PI controller with differential action at the discrete-time domain is proposed in [18], whereas the decoupling capability is not considered. In [19], the controller is designed based on the zero-pole cancellation principle in the discrete domain and realizes the full decoupling of axes d and q [20]. To improve the system damping, a virtual resistance is also added to the feedforward [21]. However, the dynamic performance of the controller for command tracking is not optimal, and the speed with which the controller can cancel the effect of a disturbance in the control loop is determined by motor parameters. In [22], a deadbeat controller with the integral function is proposed by modifying the forward path of the PI, and the controller can realize the full decoupling of axes d and q and have the deadbeat response for current reference tracking. However, the forward path of the controller contains imaginary components, which increases the complexity of the implementation. Besides, due to temperature and other reasons, the motor parameters may deviate from the nominal value, and the performance of the controller also needs further analysis. Therefore, to improve the decoupling performance and dynamic performance of the controller, especially when the parameters are inaccurate, the PI controller needs further research.

In this paper, a deadbeat PI controller with modified feedforward designed in the discrete domain is proposed to improve the performance of the current-loop. Firstly, the ZOH-equivalent discrete model is deduced with the complex vector approach. With the discrete model, the limitations of the conventional controller are obtained, including command tracking and the disturbance rejection capability. For improving the dynamic performance, by introducing three different coefficients into the feedforward, the controller can achieve full control over the location of the closed-loop poles. As a result, it can realize the deadbeat response for current reference tracking with two samples delay and ensure the full decoupling of axes d and q. Furthermore, as the motor parameters deviate from the nominal value, the controller coefficients are designed to guarantee the performance of the current-loop. Finally, the effectiveness of the proposed controller is verified by experiments.

II. DISCRETE MODEL IN SRF
In order to improve the performance of PI controller, and conveniently take the calculation delay and ZOH introduced by PWM into consideration, it is necessary to deduce the discrete model in SRF.

Since the output voltages latched by the inverter are three-phase voltage in *abc* coordinates, it is preferred to acquire the ZOH-equivalent discrete model in stationary reference frame firstly.

When the magnetic saturation, iron loss and eddy current loss are ignored, the complex vector voltage equation of PMSM in the α-β axes stationary coordinate system is

$$\frac{d\boldsymbol{i}_{\alpha\beta}}{dt} = \frac{\boldsymbol{u}_{\alpha\beta} - j\omega_{\mathrm{r}}\psi_{\mathrm{f}}e^{j\theta_{\mathrm{e}}}}{L_{\mathrm{s}}} - \frac{R_{\mathrm{s}}}{L_{\mathrm{s}}}\boldsymbol{i}_{\alpha\beta} \tag{1}$$

where $\boldsymbol{i}_{\alpha\beta}$ is the stator currents in the $\alpha - \beta$ axes stationary coordinate, and $\boldsymbol{u}_{\alpha\beta}$ is the stator voltage in the $\alpha - \beta$ axes stationary coordinate system. θ_{e} is the rotor position of PMSM. ω_{r} is the electrical rotor speed. R_{s} is the stator phase resistance of the motor. L_{s} is d or q axis inductor. ψ_{f} is the rotor flux linkage.

In the time interval $k_1 T_{\mathrm{s}}$ to $(k_1 + 1)T_{\mathrm{s}}$, the motor speed ω_{r} and the stator voltages remain constant, then

$$\begin{cases} \theta_{\mathrm{e}}(t) = \theta_{\mathrm{e}}(k_1 T_{\mathrm{s}}) + \omega_{\mathrm{r}}(t - k_1 T_{\mathrm{s}}) \\ \boldsymbol{u}_{\alpha\beta}(t) = \boldsymbol{u}_{\alpha\beta}(k_1 T_{\mathrm{s}}) \end{cases} \tag{2}$$

Combining (1) and (2), the current expression of $(k + 1)T_{\mathrm{s}}$ time could be presented as

$$\boldsymbol{i}_{\alpha\beta}[(k_1 + 1)T_s] = e^{-\frac{R_{\mathrm{s}}}{L_{\mathrm{s}}}T_{\mathrm{s}}}\boldsymbol{i}_{\alpha\beta}(k_1 T_{\mathrm{s}}) + \frac{1}{L_{\mathrm{s}}}$$
$$\times \int_{k_1 T_{\mathrm{s}}}^{(k_1+1)T_{\mathrm{s}}} e^{-\frac{R_{\mathrm{s}}}{L_{\mathrm{s}}}[(k_1+1)T_s-\tau]}$$
$$\times (\boldsymbol{u}_{\alpha\beta}(kT_s) - j\omega_{\mathrm{r}}\psi_{\mathrm{f}}e^{j\theta_{\mathrm{e}}(kT_s)+j\omega_r(\tau-kT_s)})\mathrm{d}\tau \tag{3}$$

whereby, the ZOH-equivalent discrete model in the stationary coordinate is shown as

$$\boldsymbol{i}_{\alpha\beta}[(k_1 + 1)T_s] = a\boldsymbol{i}_{\alpha\beta}(k_1 T_s) + b\boldsymbol{u}_{\alpha\beta}(k_1 T_s)$$
$$- c_{\mathrm{g}}j\omega_{\mathrm{r}}\psi_{\mathrm{f}}e^{j\theta_{\mathrm{e}}(k_1 T_s)} \tag{4}$$

where $a = e^{-\frac{R_{\mathrm{s}}}{L_{\mathrm{s}}}T_{\mathrm{s}}}$, $b = \frac{1-a}{R_{\mathrm{s}}}$ and $c_{\mathrm{g}} = \frac{e^{j\omega_{\mathrm{r}}T_s}-a}{R_{\mathrm{s}}+j\omega_{\mathrm{r}}L_{\mathrm{s}}}$.

It is worth noting that the stator voltages are constant under the inherent digital delay time, and the voltages can be present as (5).

$$\boldsymbol{u}_{\alpha\beta}[k_1 T] = \hat{\boldsymbol{u}}_{\alpha\beta}[(k_1 - 1)T_{\mathrm{s}}] \tag{5}$$

$\hat{\boldsymbol{u}}_{\alpha\beta}$ represent the voltages calculated by controller. Thus the discrete model considering digital delay is shown as

$$\boldsymbol{i}_{\alpha\beta}[(k_1 + 1)T_s] = a\boldsymbol{i}_{\alpha\beta}(k_1 T_s) + b\hat{\boldsymbol{u}}_{\alpha\beta}[(k_1 - 1)T_s]$$
$$- c_{\mathrm{g}}j\omega_{\mathrm{r}}\psi_{\mathrm{f}}e^{j\theta_{\mathrm{e}}(k_1 T_s)} \tag{6}$$

By multiplying $e^{-j\theta_{\mathrm{e}}(kT_{\mathrm{s}})}$ both sides of (6), the discrete equation in SRF is

$$\boldsymbol{i}_{dq}[(k_1 + 1)T_s] = a_{\mathrm{g}}\boldsymbol{i}_{dq}[k_1 T_s] + b_{\mathrm{g}}\hat{\boldsymbol{u}}_{dq}[(k_1 - 1)T_s]$$
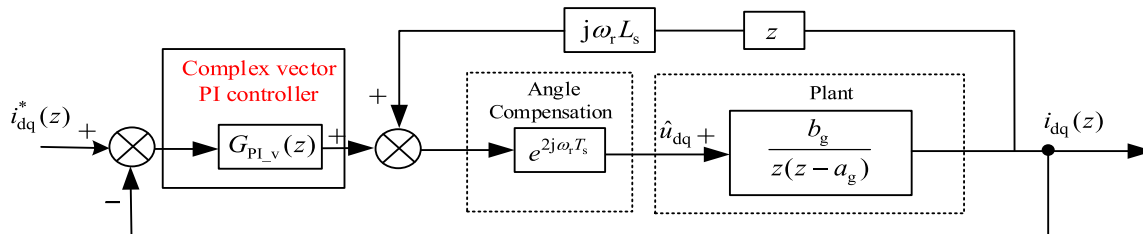$$- c_{\mathrm{g1}}j\omega_{\mathrm{r}}\psi_{\mathrm{f}} \tag{7}$$

FIGURE 1. The block diagram of the conventional complex vector PI controller.

where $a_g = ae^{-j\omega_r T_s}$, $b_g = be^{-2j\omega_r T_s}$ and $c_{g1} = c_g e^{-j\omega_r T_s}$.

From (7), the ZOH-equivalent model in SRF is obtained.

$$i_{dq}(z) = \frac{b_g}{z(z - a_g)}\hat{u}_{dq} - \frac{c_{g1}}{z - a_g}j\omega_r\psi_f \qquad (8)$$

III. LIMITATIONS OF CONVENTIONAL CURRENT CONTROLLER

To improve the performance of the controller and realize the decoupling function, $j\omega_r L_s i_{dq}$ is introduced into the feedforward term of the PI controller, and the motor model is simplified to *R-L* form in SRF. However, when the motor operates at low carrier ratio, the decoupling capability of the PI controller is limited because of time-delay [23]. The feedforward with the current prediction proposed in [24] is added to eliminate time delay. Its control block diagram in the discrete domain is shown in Fig. 1, where the voltage disturbance is ignored.

From Fig. 1, it can get the open-loop transfer function.

$$G_o^R = \underbrace{\frac{k(z - z_0)}{b(z - 1)}}_{G_{PI\_v}} \frac{b}{z(z - a\cos\omega_r T_s + ja\sin\omega_r T_s - bj\omega_r L_s)} \qquad (9)$$

where k is the proportion of the PI controller. It can be seen from (9), the impedance $j\omega_r L_s$ could not be eliminated by the j $a\sin\omega_r T_s$. As a result, the transfer function has the imaginary part, indicating that the current exists coupling components between d and q axes.

To improve the decoupling capability, it is necessary to design the zero of the PI controller. With the (10), the transfer function can eliminate the imaginary part. Meanwhile, it can be found that the zero of the PI controller contains the imaginary part, so it is a complex vector PI controller, which makes the implementation structure more complicated.

$$z_0 = a\cos\omega_r T_s - ja\sin\omega_r T_s + bj\omega_r L_s \qquad (10)$$

Combining (9) and (10), the closed-loop transfer function of system is

$$G_c^R = \frac{k}{z^2 - z + k} \qquad (11)$$

From (11), the form of the transfer function is the same as the controller in [20], and the stable range of the system is $0 < k < 1$. With $k = 0.25$, both poles are located at real axes, and

the value of closed-loop poles are satisfied (12). It can be seen from (12) that the minimum value of poles from the origin is 0.5 by adjusting the k. As a result, the dynamic performance of the complex vector PI controller is not optimal.

$$p_1 = p_2 = 0.5 \qquad (12)$$

With regard to the disturbance rejection, the transfer function is shown as

$$G_c^{RD} = -\frac{c_{g1}z(z - 1)}{(z - a_g - bj\omega_r L_s)(z^2 - z + k)} \qquad (13)$$

Compared to the characteristic polynomials of (11) and (13), we can find that the transfer function G_c^{RD} has the same poles as the G_c^R, and adds a pole located at $p = a_g + bj\omega_r L_s$. For the disturbance rejection, this pole is poorly damped because it contains the imaginary part. Therefore, the current controller has a slower response to the variation in disturbance, and the dynamic performance is determined by the parameters of PMSM.

IV. THE PROPOSED CURRENT CONTROLLER WITH MODIFIED FEEDFORWARD ITEMS

From the above, the conventional complex vector PI controller cannot realize the deadbeat response for command tracking. On the other hand, the controller cannot control the speed of disturbance elimination, and it is determined by parameters of PMSM.

To improve the performance of the system, a deadbeat PI controller is proposed by modifying the feedforward, as shown in Fig. 2. It can be seen from that the feedforward contains imaginary components, which can eliminate the imaginary component of the complex vector PI controller zero, and the implementation structure is simpler. The degree of freedom of the proposed controller can also be improved by introducing three different coefficients, which can be applied to assign locations of the poles.

A. THE PERFORMANCE OF THE COMMAND TRACKING

From Fig. 2, the open-loop transfer function of this system is

$$G_o^P = \underbrace{\frac{k(z - z_1)}{b(z - 1)}}_{G_{PI}} \frac{b}{z(z - a_g - jb\sigma - b\delta) + b\gamma} \qquad (14)$$
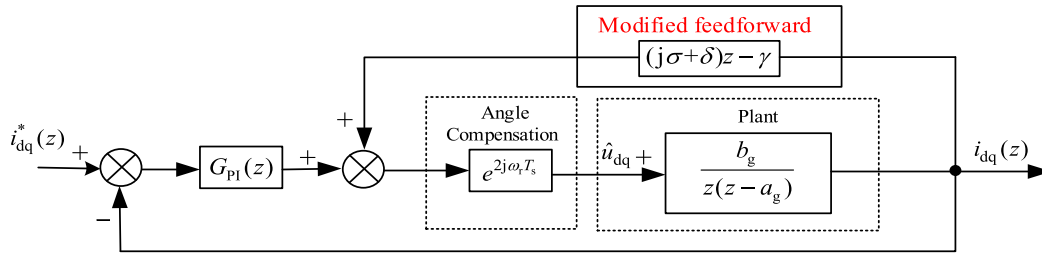
FIGURE 2. The block diagram of the proposed PI controller.

From (14), the proposed controller has three poles, and its characteristic polynomial is

$$P(z) = (z-1)[z\underbrace{(z - a_g - jb\sigma - b\delta)}_{G_A} + b\gamma] = 0 \quad (15)$$

For realizing that three poles are all on the real axis, the imaginary value of G_A is set to 0, and the σ meets

$$\sigma = \frac{a \sin(\omega_r T_s)}{b} \quad (16)$$

Combining (14) and (16), the open-loop transfer function is expressed as

$$G_o^P = \frac{k(z - z_1)}{b(z - 1)} \frac{b}{(z - a_1)(z - a_2)} \quad (17)$$

where $\delta = \frac{a_1 + a_2 - a \cos \omega_r T_s}{b}$ and $\gamma = \frac{a_1 a_2}{b}$.

From (17), it is easy to realize the decoupling function when the values of a_1 and a_2 are real, and it is also a reasonable considering that the ranges of a_1 and a_2 should satisfy $(-1 < a_1 < 1, -1 < a_2 < 1)$. At the same time, γ and δ are real numbers, and satisfy

$$\begin{cases} -\dfrac{1}{b} \le \gamma \le \dfrac{1}{b} \\ \dfrac{-2 - a \cos \omega_r T_s}{b} \le \delta \le \dfrac{2 - a \cos \omega_r T_s}{b} \end{cases} \quad (18)$$

The zero of the PI controller meets (19). It can be seen that the zero only contains the real component, and the implementation structure is simpler than that of the complex vector PI controller.

Moreover, the controller also retains the integral function, which can improve the robustness of the motor parameter changes.

$$z_1 = a_1 \quad (19)$$

With the (19), the closed-loop transfer function of system is

$$G_{cl}^P = \frac{i_{dq}(z)}{i_{dq}^*(z)} = \frac{k}{z^2 - (a_2 + 1)z + k + a_2} \quad (20)$$

The poles of the closed-loop system are seen as

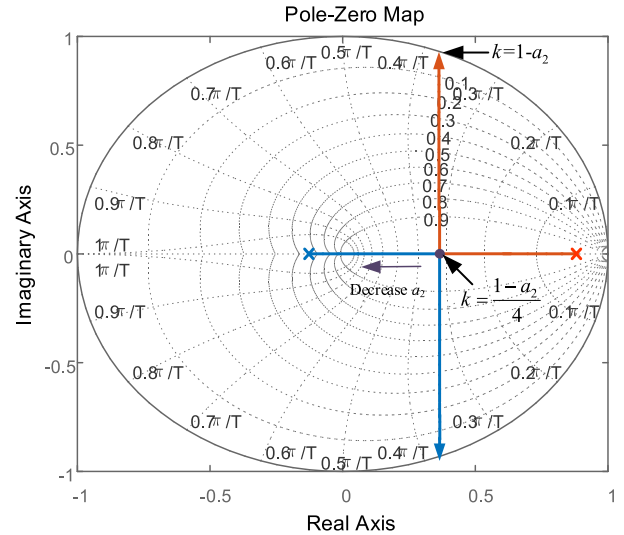$$p_{1,2} = \frac{a_2 + 1 \pm \sqrt{(a_2 + 1)^2 - 4(k + a_2)}}{2} \quad (21)$$

FIGURE 3. The closed-loop poles locations with different coefficient *k*.

From (21), it can be seen that the poles of closed-loop system could be determined by the values of a_2 and k. When $p_1 = p_2$, the corresponding k value is

$$k = \frac{(a_2 - 1)^2}{4}, \left(p_1 = p_2 = \frac{a_2 + 1}{2}\right) \quad (22)$$

When the poles reach the boundary of unit circle, the corresponding k value is

$$k = 1 - a_2, (|p_1| = |p_2| = 1) \quad (23)$$

As a result, the closed-loop poles locations with different k is shown in Fig. 3.

As shown in Fig. 3, both the two closed-loop poles are located on the real axis when the k value is satisfied with (22), which means that the controller achieves no overshoot response for command tracking. At the same time, both closed-loop poles can gradually close to the original point with decreasing a_2, indicating that the dynamic performance of current can be further improved. When $a_2 = -1$, both the two closed-loop poles are located at the origin, and the current loop reaches fastest response, which is shown as a deadbeat control system.

When $a_2 = -1$, the γ and δ can be solved.

$$\begin{cases} \gamma = \dfrac{-a_1}{b} \\ \delta = \dfrac{a_1 - 1 - a\cos\omega_r T_s}{b} \end{cases} \tag{24}$$

When $a_2 = 0$, it also can be allowed to decrease the dynamic performance of system to reduce the magnitude of controller action, and the controller coefficients are shown below

$$\begin{cases} \gamma = 0 \\ \delta = \dfrac{a_1 - a\cos\omega_r T_s}{b} \end{cases} \tag{25}$$

The closed-loop transfer function of the system is

$$G_{cl}^P = \frac{i_{dq}(z)}{i_{dq}^*(z)} = \frac{k}{z^2 - z + k} \tag{26}$$

As shown in (26), the dynamic performance of the proposed controller is the same as that of the complex vector PI controller in the discrete domain.

Therefore, only the motor parameters such as inductance and resistance are needed in the proposed controller. It can calculate the coefficients σ, δ and γ by (16) and (24). With these coefficients, the proposed controller can achieve full decoupling of d and q axes, and realize the deadbeat response. To reduce the amplitude of the controller action, it is also feasible to get the slower dynamic performance by selecting the coefficients with (25), and the dynamic performance is the same with that of the complex vector controller.

B. THE PERFORMANCE OF THE VARIATION IN PERTURBATION

The performance of the variation in perturbation will be studied from two aspects: the dynamic performance and the harmonic suppression capability.

When the controller can achieve the deadbeat tracking, the closed-loop transfer function to the disturbances is

$$G_c^D(z) = \frac{i_{dq}(z)}{j\omega_r\psi_f} = -\frac{c_{g1}z(z-1)}{z^2(z-a_1)} \tag{27}$$

From (27), it can be found that the value of $|a_1|$ determines the dynamic response to the disturbance. A smaller value of $|a_1|$ corresponds to a faster response because the pole is more close to the origin. Compared with the complex vector controller, the poles of the deadbeat PI controller only have the real component, and the dynamic performance for disturbance rejection is determined by a_1, which is not limited to the motor parameters. Therefore, the proposed deadbeat PI controller can have better response to the disturbance rejection.

In order to further study the character of the controller, the disturbance rejection capability under different a_1 is shown in Fig. 4. For a given frequency, the harmonic suppression capability will be better with smaller magnitude. It can be
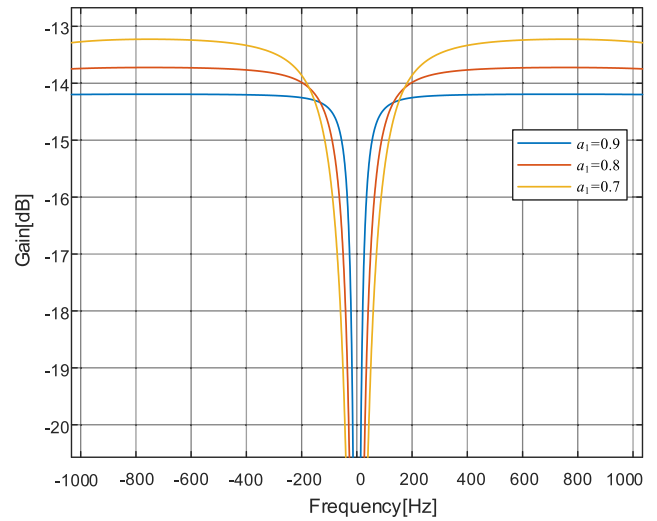
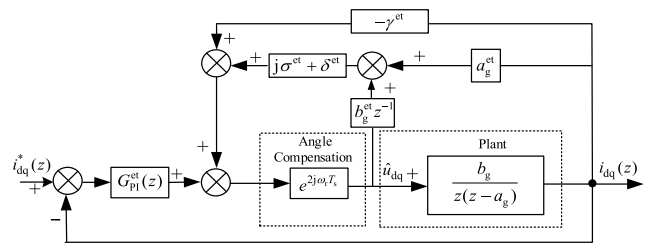**FIGURE 4.** Amplitude-frequency curves of proposed controller under different a_1.

FIGURE 5. Control block diagram of proposed controller with inaccurate inductance.

seen that increasing the $|a_1|$ improves steady-state rejection for harmonic orders exceeding 1, which is the main harmonic range for the disturbances when the motor operates at low carried ratio.

In summary, with the smaller value of $|a_1|$, the dynamic performance of system to the variation in perturbation is faster, while the rejection of harmonic noise is worse. As a result, the selection of $|a_1|$ should be a compromise between these facts.

V. THE CONTROLLER COEFFICIENTS DESIGN UNDER INACCURATE PARAMETERS

When the motor operates at high speed, the back electromotive force (EMF) and coupling component are the main influencing factors compared to resistance component. The following mainly analyses the influence of the inductance variation. Considering that the inaccurate inductance mainly affects two aspects: the prediction algorithm and the accuracy of each coefficient, the control block diagram of the proposed controller is shown in Fig. 5.

According to Fig. 5, the open-loop transfer function with inaccurate parameters is

$$G_o^{et} = \frac{(z-a_1)}{z-1} \frac{b/b^{et}}{z^2 + c_0 z + c_1} \tag{28}$$

where

$$c_0 = -a_g - b\frac{b_g^{et}}{b_g}(j\sigma^{et} + \delta^{et}),$$

$$c_1 = -b[(a_g^{et} - \frac{a_g}{b_g}b_g^{et})(j\sigma^{et} + \delta^{et}) - \gamma^{et}],$$

$$\sigma_{et} = \frac{a_{et}\sin(\omega_r T_s)}{b_{et}}, \quad \gamma_{et} = \frac{-a_1}{b_{et}},$$

$$\delta_{et} = \frac{a_1 - 1 - a^{et}\cos\omega_r T_s}{b^{et}}, \quad a_g^{et} = a^{et}e^{-j\omega_r T_s},$$

$$a_g^{et} = b^{et}e^{-j\omega_r T_s}, \quad a^{et} = e^{-\frac{R_s}{L_s^{et}}T_s}, \quad b^{et} = \frac{1 - a^{et}}{R_s}.$$

where L_s^{et} is the estimated inductance.

From (28), it is clear that the open-loop poles contain imaginary component because of inaccuracy parameters, which will decline decoupling capability of the d and q axes. In order to further understand the dynamic performance of the current loop, the closed-loop transfer function is shown as

$$G_c^{et} = \frac{(z - a_1)b}{(z^3 + d_0 z^2 + d_1 z + d_2)b^{et}} \quad (29)$$

where $d_0 = c_0 - 1$, $d_1 = c_1 - c_0 + \frac{b}{b^{et}}$,

$$d_2 = -c_1 - a_1\frac{b}{b^{et}} \quad$$

According to (29), the poles p_1, p_2 and p_3 can be solved. In this case, the poles of closed-loop transfer function to the reference tracking and the disturbance signal are the same, so the locations of poles can represent the overall dynamic performance.

First, define a simple index, the maximum Absolute Value of the Poles (AVP.max), to evaluate the performance of the system.

$$\text{AVP.max} = \max\{|p_1|, |p_2|, |p_3|\} \quad (30)$$

It can be found from (30) that the system is stable when AVP.max <1, and it is more stable with the smaller AVP.max. By limiting AVP.max to a certain range, it can guarantee the natural frequencies and damping factors of the poles, and the dynamic response can be avoided to be too slow or severe when the parameters of motor are mismatched.

The contour map of AVP.max with different L_s^{et} and a_1 is shown in Fig. 6. It can be seen that when the estimated inductance L_s^{et} is equal to the actual inductance L_s, the value of AVP.max is equal to a_1. Therefore, it can be found that from (29) the closed-loop transfer function can realize the zero-pole cancellation, and it is beneficial for the command tracking.

When $L_s^{et} > 1.5L_s$ or $L_s^{et} < 0.4L_s$, AVP.max can be reduced by increasing a_1 value, indicating that it can improve stability and increase dynamic response ability as well, and it is advantageous to choose a larger a_1. When $0.4L_s < L_s^{et} < 1.5L_s$, increasing a_1 can make AVP.max firstly reduce and then increase, and it is inverse to the dynamic performance.

FIGURE 6. The contour map of the AVP.max with different L_s^{et} and a_1.

FIGURE 7. AVP.max with respect to a_1 when $L_s^{et} = 1.5L_s$.

Therefore, it is necessary to further analyze the selection of a_1. Meanwhile, the stable boundary shows that the system can tolerate larger parameter errors with larger a_1.

Considering that the inductance variation range is 50%, the influence of a_1 versus the AVP.max is studied under a specific L_s^{et} ($L_s^{et} = 1.5L_s$), as shown in Fig. 7. When $a_1 = 0.71$, the AVP.max reaching the minimum value, indicating that the dynamic performance is fastest. However, due to the weak ability to suppress high-frequency noise, it is easy to cause the control saturation or torque ripple. When selecting $a_1 = 0.9$, the AVP.max is equal to a_1. It can be seen from (29) that the zero $z = a_1$ can approximately achieve the zero-pole cancellation with the maximum pole, which is beneficial to the dynamic performance of the system.

In order to verify the above theory, it further acquires the pole locations under the different estimated inductances, as shown in Fig. 8. It can be seen that the variation range of p_1 and p_2 is larger than that of p_3 in the process of
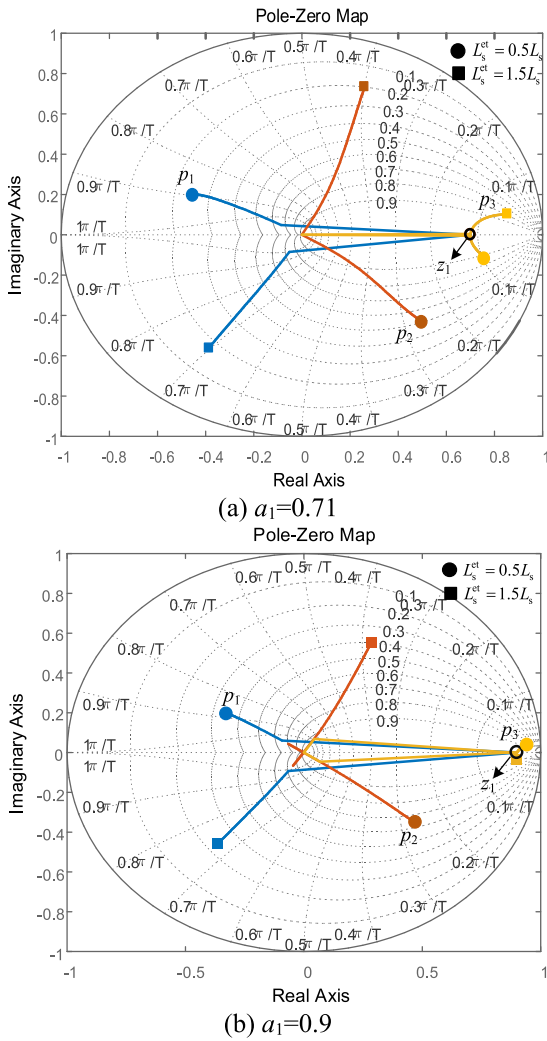
(a) a_1=0.71

(b) a_1=0.9

FIGURE 8. The closed-loop poles locations under the different estimated inductances.

TABLE 1. Model parameters of permanent magnet synchronous motor.

Symbol	Parameter	Value
p	pole pairs	4 *pair*
ψ_f	rotor flux linkage	0.12 Wb
R_s	stator phase resistance	1.345 Ω
L_s	d or q-axes inductance	3.1 mH
ω_r	rated speed	2500 r/min
P_N	rated power	1 kW
I_N	rated current	4 A

FIGURE 9. Simulation results of d and q-axes currents response for command tracking.

(a) a_1=0.8

(b) a_1=0.9
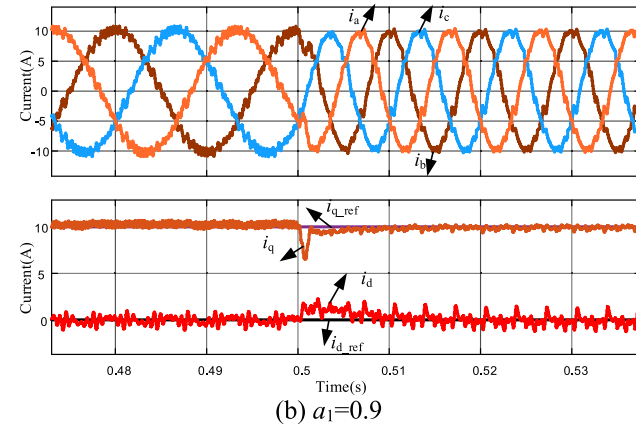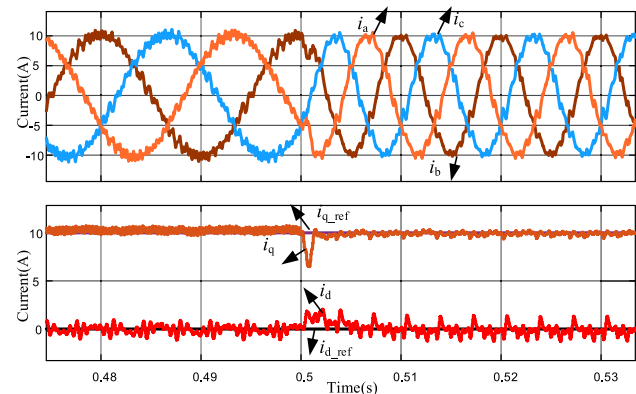
FIGURE 10. Simulation results of d and q-axes currents response for disturbance rejection under different speeds.

estimated inductance variation, meaning that p_1 and p_2 are sensitive to the parameters variation. Compared with $a_1 = 0.71$, the imaginary component of p_3 is closer to zero with $a_1 = 0.9$, and it can approximately realize the zero-pole cancellation. As a result, the dynamic performance with $a_1 = 0.9$ is better because of AVP.max reduction. Besides, the system damping is mainly determined by p_2, because it has a larger imaginary component. As shown in Fig. 8,

when $a_1 = 0.9$, the variation range of p_2 with the inductance variation is less than that of $a_1 = 0.71$, indicating that the selecting $a_1 = 0.9$ reduces the sensitivity to the inductance variation. At the same time, the imaginary part is smaller with $a_1 = 0.9$, and it can improve the system damping.

Therefore, when the inductance deviates from the nominal value, selecting $a_1 = 0.9$ can improve the dynamic performance of the current loop.

(a) a_1=0.8

(b) a_1=0.9
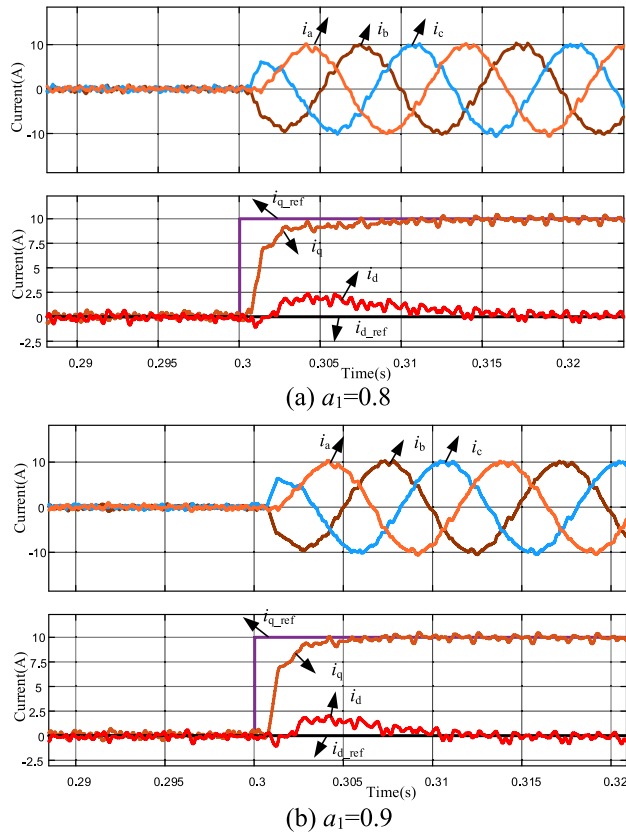
FIGURE 11. Simulation results of *d* and *q*-axes currents response with inaccurate inductance.

VI. SIMULATION RESULTS

A. SIMULATION RESULTS WHEN THE MOTOR PARAMETERS ARE ACCURATE

In order to verify the performance of the proposed controller, simulations are carried out using MATLAB/Simulink. The motor parameters are shown in Table 1. The motor speed is set to 1500r/min, and the coefficient a_1 is set to 0.9. Fig. 9 shows the simulation results of *d* and *q*-axes currents response for command tracking. Firstly, the motor operates at no load, and the currents are all around 0. At 0.3s, the reference of the *q*-axis current is set to 10A, which is about two times the rated current, and the speed remains unchanged. It can be seen that the *q*-axis current reached the command value in two samples without the overshoot and oscillation, so the proposed controller is a deadbeat PI controller. At the same time, the *d*-axis current is almost not affected, indicating that the controller realizes the full decoupling of the *d* and *q* currents, and it can guarantee that the flux component is not affected by the toque changing, and vice versa.

Furthermore, the rejection disturbance capability of the controller is validated. The voltage disturbance generally comes from the changes of the back electromotive force, so the sudden change of speed is set to verify the rejection disturbance capability and the mechanical inertia is low. The minimum and maximum speeds of the motor are set to
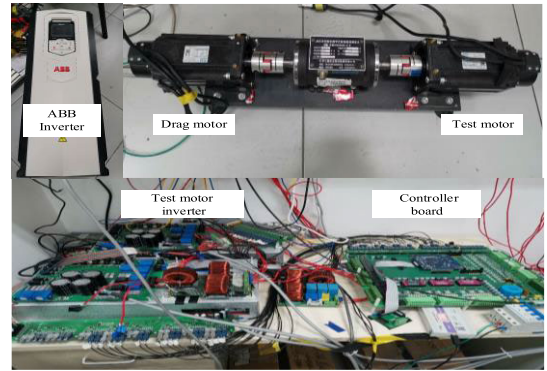
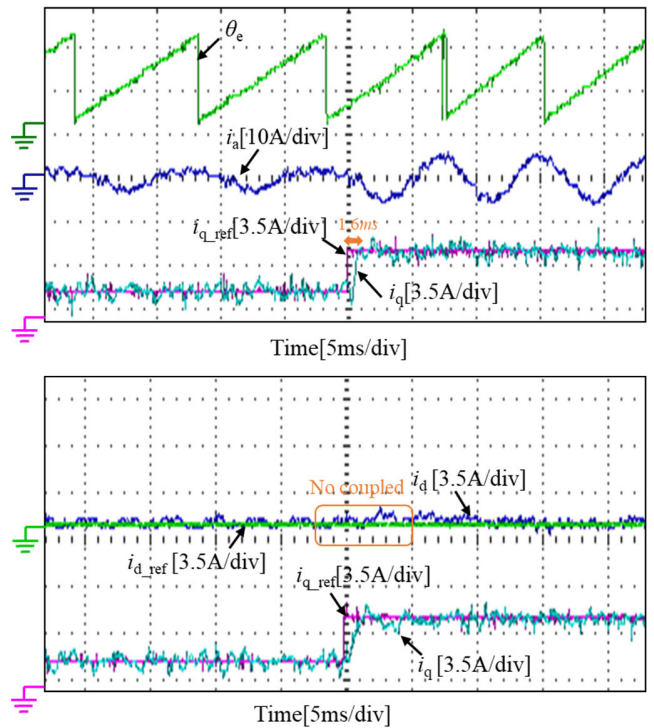**FIGURE 12.** Test platform of 1kW PMSM.

FIGURE 13. Experiment results of *d* and *q*-axes currents response for command tracking.

750r/min and 1500r/min respectively, and the response of the *d* and *q*-axes currents are observed, as shown in Fig. 10. It can be seen that the speed stepped from 750r/min to 1500r/min at 0.5s, and it causes the *d* and *q*-axes currents to generate a transient current that deviates from the reference current. For comparison, the a_1 is set to 0.8 and 0.9, respectively. From the Fig. 10, it is clear that it has better harmonic suppression capability with $a_1 = 0.9$ than that of $a_1 = 0.8$. While the speed to cancel the effect of a disturbance is faster with $a_1 = 0.8$ than that of $a_1 = 0.9$. As a result, the controller allows us to select the speed with which the controller can eliminate the effect of a disturbance. The results are well accorded with the above theoretical analysis.
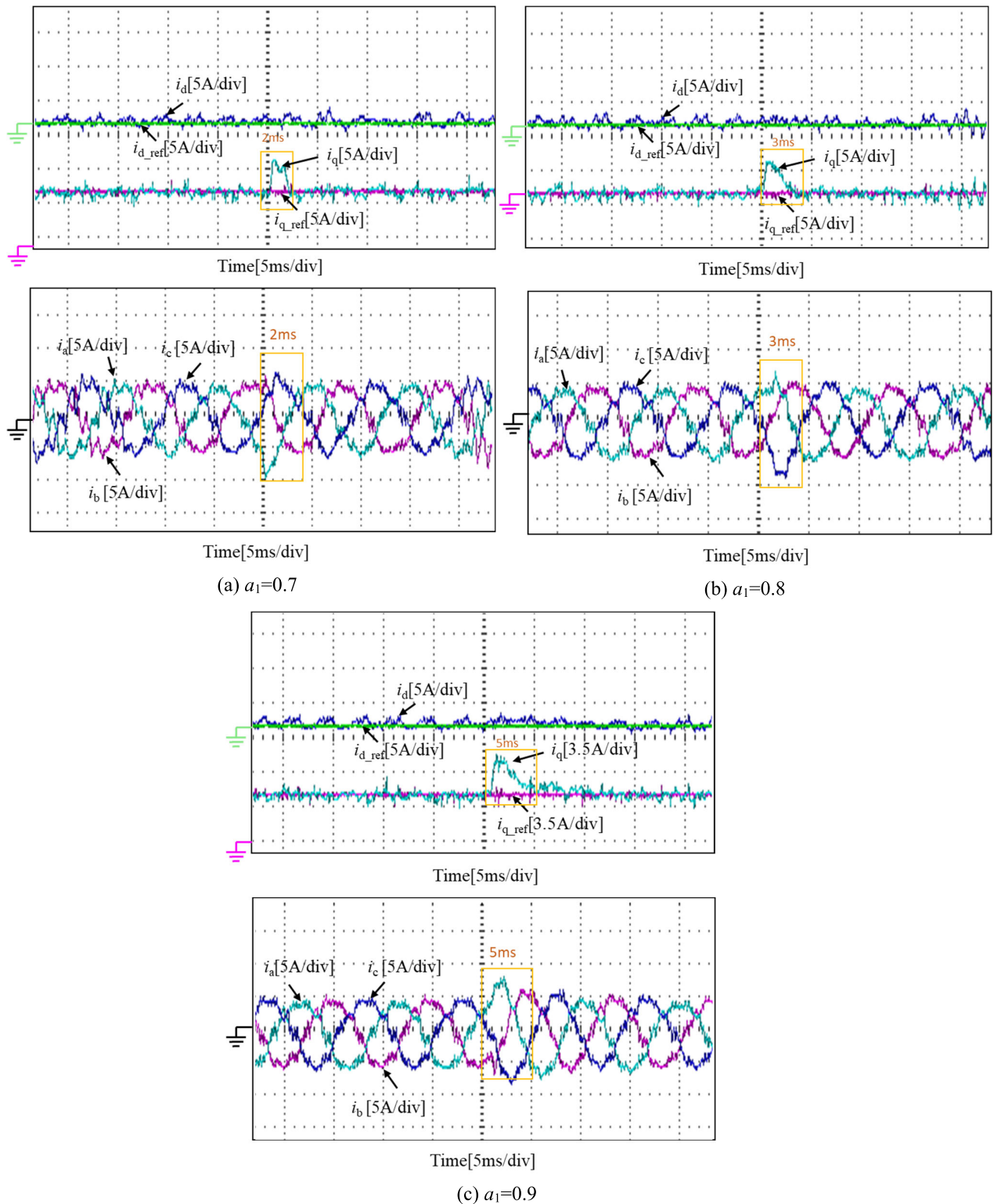
FIGURE 14. Experiment results of *d* and *q*-axes currents response for disturbance rejection.

B. SIMULATION RESULTS WHEN THE INDUCTANCE DEVIATES FROM THE NOMINAL VALUE

In practical operation, the inductance often deviates from the rated value due to the influence of temperature and magnetic field saturation. Therefore, in the simulation, the motor inductance is set to 1.5 times the rated value, and the motor speed is set to 1500r/min to observe the dynamic performance of the controller. For comparison, the a_1 is set to 0.8 and 0.9,

respectively, and the simulation results of d and q-axes currents response are shown in Figure 11. It can be seen that the command of the q-axis current is set from 0A step to 10A at 0.3s, and there is a coupling between the d and q-axes currents due to the inaccurate inductance. When $a_1 = 0.9$, the q-axis current can realize the command tracking within 5ms, and the d-axis current realizes the command tracking within 10ms. And there is no overshoot and oscillation in the process of dynamic response. From the Fig. 11, the performance of the controller under $a_1 = 0.9$ is significantly better than that of $a_1 = 0.8$ when the motor parameters are not accurate. As a result, selecting $a_1 = 0.9$ is a better choice when the inductance deviates from the nominal value.

VII. EXPERIMENT RESULTS

A. EXPERIMENT RESULTS WHEN THE MOTOR PARAMETERS ARE ACCURATE

The proposed controller based on the discrete domain is also validated on a 1kW PMSM, as shown in Fig. 12. The nameplate data are same as simulation. The DSPF28377 is used to execute the proposed method with 667us periods. The d, q currents, and the rotor position were captured from the AD7841ASZ chip that can achieve the Digital-to-Analogue Conversion. In order to make the motor operate at low carrier ratio, the speed of the motor and the switching frequency of the inverter are set to 1500r/min and 1.5 kHz, respectively. At the same time, the carrier ratio is 15. All experiments are carried out in the operation of encoderless control. And the stator voltages, currents, and the speed of the motor are used to calculate the rotor position.

When the motor parameters are accurate, the a_1 is set to 0.9, and δ, σ, and γ are solved by (16) and (24). Firstly, the dynamic performance of the controller is verified. During the actual operation, since the friction torque and the inverter capacity are limited, the minimum and maximum values of the q-axis current are set to 2A and 5A, respectively. Fig. 13 shows the waveforms of the rotor position, the currents of phase a and d, q-axes of reference and actuality. It can be seen from that the q-axis current can reach the command value in two samples when the q-axis reference was stepped, and the d-axis current is basically not affected. Therefore, the proposed controller can realize the deadbeat response for command tracking, and offer full decoupling between d and q-axes currents.

Furthermore, the rejection disturbance capability of the controller is validated. Due to the limitation of motor inertia, the motor speed changes slowly. Therefore, to verify rejection disturbance capability when the parameters are accurate, the controller is tested by injecting a step disturbance of 20V into the q-axis voltage, and it also causes the q-axis current to generate a transient current that deviates from the reference current. The experimental waveforms of the d, q-axes currents of reference and actuality and the currents of the a, b and c phase are presented in Fig. 14. In both figures, it can be seen that the d-axis current is almost unaffected by the q-axis disturbance voltage which can prove that the proposed
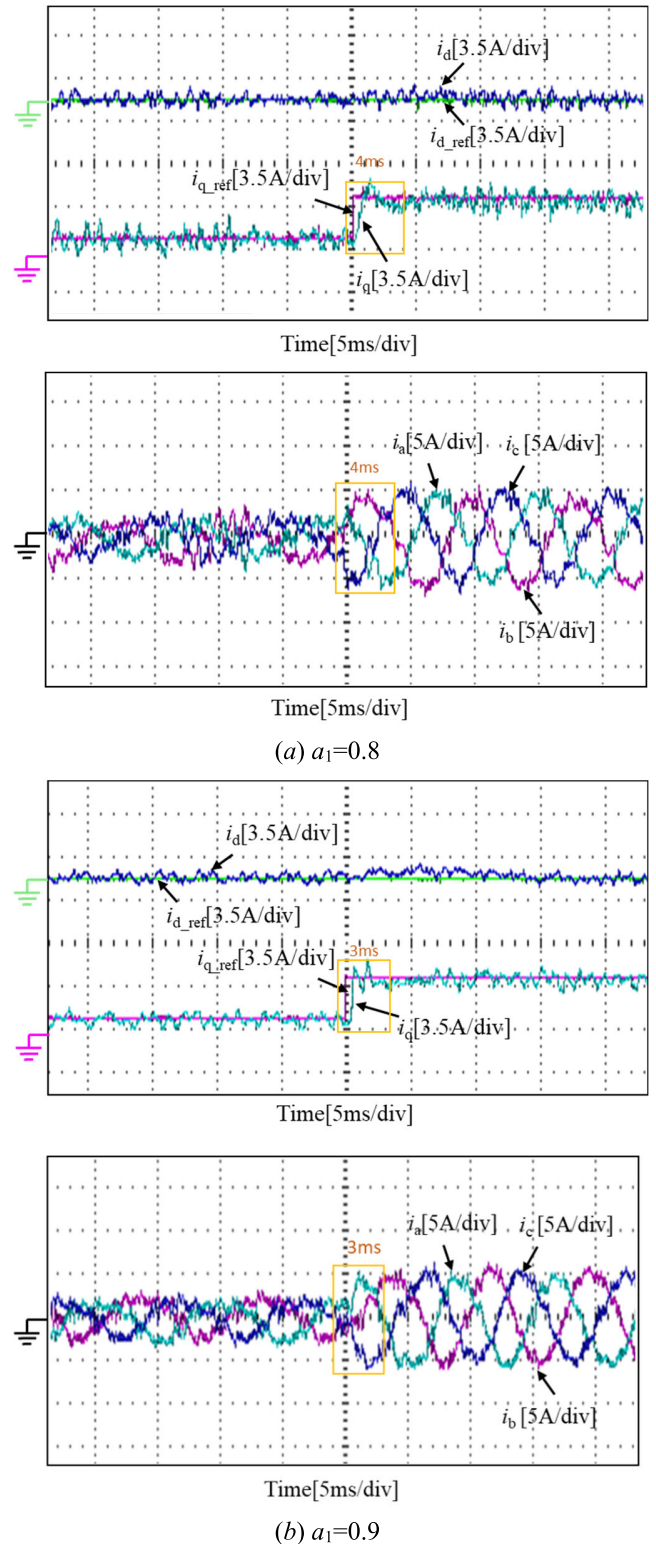

(a) a_1=0.8

(b) a_1=0.9

FIGURE 15. Experiment results of d and q-axes currents response for command tracking when $L_s^{et} = 1.5L_s$.

controller can realize the full decoupling of the d and q axes from another side. For comparison, the a_1 is set to 0.7, 0.8 and 0.9, respectively. It can be seen that when $a_1 = 0.9$, its steady-state harmonic characteristic is the best, which can
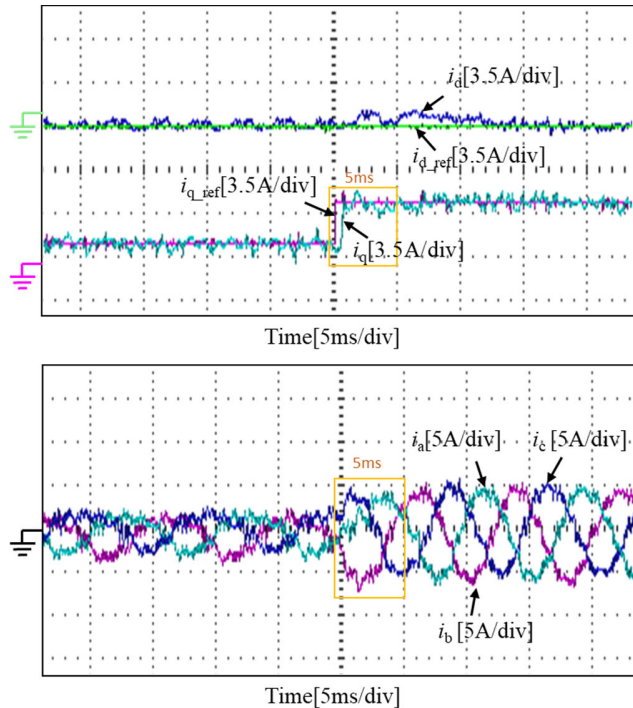
FIGURE 16. Experiment results of *d* and *q*-axes currents response for command tracking when $i_d = -1A$.

reduce torque ripple, while the speed of disturbance elimination is slow. At $a_1 = 0.7$, the speed of disturbance elimination is the fastest, and the disturbance can be eliminated in 2-3 control period, while the steady-state harmonics are larger. Therefore, the proposed deadbeat PI controller can control the speed of disturbance elimination, and the a_1 value can be selected according to the actual operating conditions.

B. EXPERIMENT RESULTS WHEN THE INDUCTANCE DEVIATES FROM THE NOMINAL VALUE

To make the motor operates at the condition of inaccurate parameters, the estimated inductance is set to 1.5 times the nominal value, and the motor speed is 1500r/min.

When $a_1 = 0.71$, the controller cannot operate stably because of the low Signal to Noise Ratio (SNR), as a result we select $a_1 = 0.8$ and $a_1 = 0.9$ for comparison. As shown in Fig. 15, the currents have a large number of harmonics due to the inaccuracy of the inductance. Therefore, choosing a larger a_1 can have better harmonic suppression. From Fig. 15 (b), it can be seen from that when $a_1 = 0.9$, the q-axis current can realize the command tracking within 3ms, and it has better dynamic performance than that of $a_1 = 0.8$, which is mainly due to the decrease of AVP.max. So the experimental results are consistent with the theoretical analysis.

In the actual application, the inductance is mainly affected by temperature and magnetic field. Therefore, set the d-axis current to $-1A$, which is about 20% of the rated current, and the inductance will increase because of the air-gap flux reducing. As shown in Fig. 16, when the reference of the q-axis current was stepped from

2A to 5A at $a_1 = 0.9$, it can be seen that the q-axis current can realize the command tracking within 5ms, and there is less overshoot. Therefore, it can meet the dynamic response requirement.

VIII. CONCLUSION

This paper mainly proposed a deadbeat PI controller under the discrete domain when the motor operates at low carrier ratio. The proposed controller can realize the deadbeat response and offer the full decoupling between d and q axes. For reducing the magnitude of the controller, it is also feasible to achieve the same dynamic performance as the complex vector controller by designing coefficients. For the disturbance rejection, the proposed controller can realize the control of the dynamic performance, and it allowed that the controller is quick to cancel disturbances. When the inductance is inaccurate, the controller coefficients design is also considered in this paper. By combing the maximum absolute value of the poles, it can be found that choosing a larger a_1 can improve the dynamitic performance and harmonic suppression capability of the system simultaneously. Finally, the simulations and experiments demonstrate the correctness of the above conclusions.

REFERENCES

[1] Z. Yin, L. Gong, C. Du, J. Liu, and Y. Zhong, "Integrated position and speed loops under sliding-mode control optimized by differential evolution algorithm for PMSM drives," *IEEE Trans. Power Electron.*, vol. 34, no. 9, pp. 8994–9005, Sep. 2019.

[2] G. Wang, X. Hao, N. Zhao, G. Zhang, and D. Xu, "Current sensor fault-tolerant control strategy for encoderless PMSM drives based on single sliding mode observer," *IEEE Trans. Transport. Electrific.*, vol. 6, no. 2, pp. 679–689, Jun. 2020.

[3] H. Zhang, W. Liu, Z. Chen, G. Luo, J. Liu, and D. Zhao, "Asymmetric space vector modulation for PMSM sensorless drives based on square-wave voltage-injection method," *IEEE Trans. Ind. Appl.*, vol. 6, no. 2, pp. 679–689, Jun. 2020.

[4] Z. Chen, H. Zhang, W. Tu, G. Luo, D. Manoharan, and R. Kennel, "Sensorless control for permanent magnet synchronous motor in rail transit application using segmented synchronous modulation," *IEEE Access*, vol. 7, pp. 76669–76679, 2019.

[5] H. Yang, Y. Zhang, G. Yuan, P. D. Walker, and N. Zhang, "Hybrid synchronized PWM schemes for closed-loop current control of high-power motor drives," *IEEE Trans. Ind. Electron.*, vol. 64, no. 9, pp. 6920–6929, Sep. 2017.

[6] C. Wang, K. Wang, and X. You, "Research on synchronized SVPWM strategies under low switching frequency for six-phase VSI-fed asymmetrical dual stator induction machine," *IEEE Trans. Ind. Electron.*, vol. 63, no. 11, pp. 6767–6776, Nov. 2016.

[7] B. P. McGrath, S. G. Parker, and D. G. Holmes, "High-performance current regulation for low-pulse-ratio inverters," *IEEE Trans. Ind. Appl.*, vol. 49, no. 1, pp. 149–158, Jan. 2013.

[8] A. G. Yepes, A. Vidal, O. López, and J. Doval-Gandoy, "Evaluation of techniques for cross-coupling decoupling between orthogonal axes in double synchronous reference frame current control," *IEEE Trans. Ind. Electron.*, vol. 61, no. 7, pp. 3527–3531, Jul. 2014.

[9] A. G. Yepes, A. Vidal, J. Malvar, O. López, and J. Doval-Gandoy, "Tuning method aimed at optimized settling time and overshoot for synchronous proportional-integral current control in electric machines," *IEEE Trans. Power Electron.*, vol. 29, no. 6, pp. 3041–3054, Jun. 2014.

[10] D. G. Holmes, B. P. McGrath, and S. G. Parker, "Current regulation strategies for vector-controlled induction motor drives," *IEEE Trans. Ind. Electron.*, vol. 59, no. 10, pp. 3680–3689, Oct. 2012.

[11] M. Hinkkanen, H. A. A. Awan, Z. Qu, T. Tuovinen, and F. Briz, "Current control for synchronous motor drives: Direct discrete-time pole-placement design," *IEEE Trans. Ind. Appl.*, vol. 52, no. 2, pp. 1530–1541, Mar./Apr. 2016.

[12] M. D. Soricellis, D. D. Ru, and S. Bolognani, "A robust current control based on proportional-integral observers for permanent magnet synchronous machines," *IEEE Trans. Ind. Appl.*, vol. 54, no. 2, pp. 1437–1447, Mar. 2018.

[13] A. G. Yepes, F. D. Freijedo, Ó. Lopez, and J. Doval-Gandoy, "High-performance digital resonant controllers implemented with two integrators," *IEEE Trans. Power Electron.*, vol. 26, no. 2, pp. 563–576, Feb. 2011.

[14] B.-H. Bae and S.-K. Sul, "A compensation method for time delay of full-digital synchronous frame current regulator of PWM AC drives," *IEEE Trans. Ind. Appl.*, vol. 39, no. 3, pp. 802–810, May/Jun. 2003.

[15] J. Holtz, J. Quan, J. Pontt, J. Rodriguez, P. Newman, and H. Miranda, "Design of fast and robust current regulators for high-power drives based on complex state variables," *IEEE Trans. Ind. Appl.*, vol. 40, no. 5, pp. 1388–1397, Sep. 2004.

[16] F. B. del Blanco, M. W. Degner, and R. D. Lorenz, "Dynamic analysis of current regulators for AC motors using complex vectors," *IEEE Trans. Ind. Appl.*, vol. 35, no. 6, pp. 1424–1432, Nov./Dec. 1999.

[17] H. Kim, M. W. Degner, J. M. Guerrero, F. Briz, and R. D. Lorenz, "Discrete-time current regulator design for AC machine drives," *IEEE Trans. Ind. Appl.*, vol. 46, no. 4, pp. 1425–1435, Jul./Aug. 2010.

[18] S. N. Vukosavić and L. S. Perić, "Modified digital current controller with reduced impact of transport delays," *IET Electr. Power Appl.*, vol. 10, no. 6, pp. 517–525, Jul. 2016.

[19] N. Hoffmann, F. W. Fuchs, M. P. Kazmierkowski, and D. Schröder, "Digital current control in a rotating reference frame—Part I: System modeling and the discrete time-domain current controller with improved decoupling capabilities," *IEEE Trans. Power Electron.*, vol. 31, no. 7, pp. 5290–5305, Jul. 2016.

[20] C. A. Busada, S. G. Jorge, and J. A. Solsona, "Comments on 'digital current control in a rotating reference frame—Part I: System modeling and the discrete time-domain current controller with improved decoupling capabilities,'" *IEEE Trans. Power Electron.*, vol. 34, no. 3, pp. 2980–2984, Mar. 2019.

[21] Y. Liao, F. Li, H. Lin, and J. Zhang, "Discrete current control with improved disturbance rejection for surface-mounted permanent magnet synchronous machine at high speed," *IET Electr. Power Appl.*, vol. 11, no. 7, pp. 1333–1340, Aug. 2017.

[22] C. A. Busada, S. G. Jorge, and J. A. Solsona, "A synchronous reference frame PI current controller with dead beat response," *IEEE Trans. Power Electron.*, vol. 35, no. 3, pp. 3097–3105, Mar. 2020.

[23] Q. Xiao, F. Tang, Z. Xin, J. Zhou, P. Chen, and P. C. Loh, "Large time-delay decoupling and correction in synchronous complex-vector frame," *IET Power Electron.*, vol. 12, no. 2, pp. 254–266, Feb. 2019.

[24] J.-S. Yim, S.-K. Sul, B.-H. Bae, N. R. Patel, and S. Hiti, "Modified current control schemes for high-performance permanent-magnet AC drives with low sampling to operating frequency ratio," *IEEE Trans. Ind. Appl.*, vol. 45, no. 2, pp. 763–771, Mar./Apr. 2009.

ZHIJIAN ZHANG received the B.S. degree in electrical engineering and automation from the North University of China, China, in 2018. He is currently pursuing the M.S. degree in electrical engineering from Beijing Jiaotong University. His current research interest includes advanced control of permanent magnet synchronous motor drive.

LONG JING received the B.S., M.S., and Ph.D. degrees in electrical engineering from Beijing Jiaotong University, Beijing, China, in 2000, 2002, and 2008, respectively. He is currently an Associate Professor with the Department of Electrical Engineering, Beijing Jiaotong University. His current research interests include renewable energy generation systems, microgrid, modular multilevel converters, dc grids, and power electronics for high-voltage direct current applications.

XUEZHI WU (Member, IEEE) received the B.S. and M.S. degrees in electrical engineering from Beijing Jiaotong University, Beijing, China, in 1996 and 1999, respectively, and the Ph.D. degree in electrical engineering from Tsinghua University, Beijing, in 2002. He is currently an Associate Professor with the Department of Electrical Engineering, Beijing Jiaotong University. His current research interests include microgrids, wind power generation systems, power converters for renewable generation systems, power quality, and motor control.

WENZHENG XU received the B.Eng. degree in electrical engineering from Beijing Jiaotong University in 2012, the M.Sc. degree (Hons.) in energy engineering from The University of Hong Kong, in 2013, and the Ph.D. degree in electrical engineering from The Hong Kong Polytechnic University (PolyU), in 2020. From September 2013 to June 2015, he was a Research Assistant with the Department of Electrical Engineering, PolyU, working on high-power converters and fast-charging devices for electric vehicles, where he was a Postdoctoral Fellow, from March 2020 to June 2020. He is currently a Lecturer with the School of Electrical Engineering, Beijing Jiaotong University. His research interests include power electronics, wireless power transfer, transportation electrification, and energy interconnection.

JINGDOU LIU received the B.S. and M.S. degrees in electrical engineering from Beijing Jiaotong University, Beijing, China, in 1999 and 2006, respectively. He is currently a Senior Engineer with the Department of Electrical Engineering, Beijing Jiaotong University. His current research interests include multilevel converters, power quality, and renewable power generation.

GEGE LYU received the B.S. degree in electrical engineering and automation from Beijing Jiaotong University, in 2019, where she is currently pursuing the M.S. degree in electrical engineering. Her current research interest includes impedance detection of DC distribution systems.
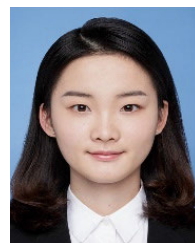
ZILIAN FAN received the B.S. degree in electrical engineering and automation from the Nanjing University of Science and Technology, Nanjing, China, in 2019. She is currently pursuing the M.S. degree in electrical engineering with Beijing Jiaotong University. Her current research interests include modeling and control of wireless power transfer and power electronics.

• • •